materials

MDPI

Letter

The Structure, Vibrational Spectra, and Thermal Expansion Study of AVO_4 (A=Bi, Fe, Cr) and $Co_2V_2O_7$

Xiaoke He [1,*], Chenjun Zhang [2,3] and Ding Tian [1]

1 School of Electric Power, North China University of Water Resources and Electric Power, 450045, China; 18848968152@163.com
2 National Research Center of Pumps, Jiangsu University, Zhenjiang, 212013, China; zcj5503@163.com
3 School of Mechanical Engineering, Luoyang Institute of Science and Technology, Luoyang, 471023, China
* Correspondence: hexiaoke@ncwu.edu.cn

Received: 9 February 2020; Accepted: 27 March 2020; Published: 1 April 2020

Abstract: Vanadate is an important functional material. It has been widely studied and applied in luminescence and photocatalysis. Vanadium compounds have been synthesized to investigate the thermal expansion properties and structure. Both $BiVO_4$ and $Co_2V_2O_7$ are monoclinic at room temperature, $FeVO_4$'s crystal structure is triclinic, and $CrVO_4$ is orthorhombic. The relatively linear, thermal-expansion, and temperature-dependent Raman spectroscopy results showed that the phase transition of $BiVO_4$ occurred at 200 to 300 °C. The coefficient of thermal expansion (CTE) of $Co_2V_2O_7$ was larger than that of the monoclinic structure $BiVO_4$. The CTE of the tetragonal structure of $BiVO_4$ was 15.27×10^{-6} °C^{-1} which was the largest CTE in our measurement results, and the CTE of anorthic structure $FeVO_4$ was 2.84×10^{-6} °C^{-1} and was the smallest.

Keywords: vanadium; Raman spectroscopy; thermal expansion; crystal structure

1. Introduction

Due to the multivalent of vanadium, vanadate has rich physical and chemical properties. Vanadate is a kind of important functional material; it has been widely studied and applied in luminescence and photocatalysis. The bandgap of $BiVO_4$ is approximately 2.0 eV which means that it is a classic semiconductor. Bidmuth vanadate ($BiVO_4$) is a polycrystalline compound, among which there are three kinds of crystal structures: monoclinic, orthorhombic, and tetragonal structure. The tetragonal structure has absorption band in the ultraviolet region, while the monoclinic structure has absorption band in the visible region as well as in the ultraviolet region. Vanadate ($BiVO_4$) has emerged as a very photoanode for photoelectrochemical water splitting [1–5]. Although the hole/electron pair, produced by the excitation of $BiVO_4$, has strong redox ability; it also has some disadvantages for practical application: a high electron hole recombination rate, low photocatalytic efficiency, small particles which are easy to lose and difficult to recover, etc. As an n-type semiconductor material, the bandgap of $FeVO_4$ is approximately 1.9–2.7 eV. There are four crystal types of $FeVO_4$, only triclinic structure material is easy to obtain [6]. The triclinic structure of $FeVO_4$ remains up to approximately 3 GPa, and then a first-order phase transition to a new monoclinic with space group C2/m is observed [7]. As a kind of transition metal oxide, $FeVO_4$ can be used as electrode materials for ion batteries and supercapacitors [8–11]. The compound materials of $FeVO_4/BiVO_4$ and $FeVO_4/V_2O_5$ has higher than pure $FeVO_4$ photocatalytic activity [12,13]. Chrome vanadate has three different crystal forms tetragonal, monoclinic, and orthorhombic structures [7]. The ambient-pressure stable polymorph of $CrVO_4$ is orthorhombic space group D_{2h}^{17}-Cmcm-, with Z=4 at room temperature [14]. Cobalt vanadates and their composites have drawn a tremendous amount of attention because of their outstanding cycling stability [15,16]. The $Co_2V_2O_7$ was recently reported to exhibit amazing magnetic field-induced

magnetization plateaus and ferroelectricity, but its magnetic ground state remains ambiguous due to the fact of its structural complexity [17].

From the above discussion, we know that vanadium compounds have many structures, rich physical and chemical properties which makes them have potential application value in many aspects. Although there are many studies on the structure and application of vanadium compounds, the thermal expansion of materials has not been reported very intensively. It has been pointed out that ionic radius and electronegativity of the cations are important with respect to structure and phase transition temperature [18,19]. Herein, we have prepared some vanadate materials by a simple solid-phase sintering method, X-ray diffraction (XRD) was used to measure the structure of materials, Raman scattering was used to measure the lattice vibration, and dilatometers was used to measure the thermal expansion.

2. Experimental and Methods

The AVO_4 and $Co_2V_2O_7$ were synthesized by a solid-state method from Fe_2O_3 (≥99.0%), Bi_2O_3 (≥99.0%), Cr_2O_3 (≥99.0%), Co_2O_3 (≥99.5%), and V_2O_5 (≥99.0%). The raw materials were mixed according to stoichiometric amounts (1:1) of A_2O_3 and 2%–5% excess V_2O_5 of desirable material except (in order to compensate for the loss in the sintering process) and ground in a mortar for 2 h. Then, alcohol was poured over the raw material and grind again until dry. Lastly, it was pressed into tablets with a length of approximately 7 mm and a diameter of approximately 6 mm, followed by sintering at 750 °C for 4 h and cooling naturally to room temperature.

The XRD measurements were carried out with an X'Pert PRO X-ray Diffractometer (Bruker D8, Bruker, Karlsruhe, Germany). Raman spectroscopy (Renishaw MR-2000 Raman spectrometer, Gloucestershire, UK) with a TMS 94 heating/freezing stage with an accuracy of ±0.1 °C was used to characterize the vibrational property of lattice. The linear thermal expansion coefficients were measured on dilatometers (LINSEIS DIL L76, Linseis, Selb, Germany), with heating and cooling rates of 5 °C/min.

3. Results and Discussion

3.1. Crystal Structure Analysis

Figure 1 shows the XRD patterns of as-prepared materials. Figure 1a is the pattern of $BiVO_4$, all diffraction peaks corresponded to $BiVO_4$ (PDF No. 01-083-1699) which means that the material crystals were in monoclinic structure space group I2/b, with Z = 4. The lattice constants of $BiVO_4$ were a = 5.196 Å, b = 5.094 Å, c = 11.703 Å and $\alpha = \beta = 90°$, $\gamma = 90.380°$. Figure 1b is the pattern of $CrVO_4$, the primary diffraction peaks corresponded to $CrVO_4$ (PDF No. 00-038-1376, space group Amam) except for weak peaks indicated as "∇" for secondary phase Cr_2O_3 and "⁎" for secondary phase V_2O_5 which could relate to the fact that the reaction time was much shorter than that reported in the literature (122 h). There was a second and third phase which could lead to some situations, such as internal stress, many cracks on the tablet, etc. The material crystals in orthorhombic structure with space group Amam from the primary diffraction peaks. The lattice constants of $CrVO_4$ are a = 5.567 Å, b = 8.210 Å, c = 5.975 Å. The pattern of $FeVO_4$ is shown in Figure 1c. As seen, the diffraction peaks are corresponding to $FeVO_4$ (PDF No. 00-038-1372, space group P-1) which crystal in anorthic structure. The lattice constants of $FeVO_4$ are a = 6.720 Å, b = 8.059 Å, c = 9.256 Å, and $\alpha = 96.7°$, $\beta = 106.4°$, $\gamma = 101.6°$. Figure 1d is the pattern of $Co_2V_2O_7$, all diffraction peaks corresponded to $Co_2V_2O_7$ (PDF No. 01-070-1189) with lattice constants a = 6.595 Å, b = 8.380 Å, and c = 9.470 Å which means that the material crystals were in monoclinic structure space group P21/c, with Z = 4.

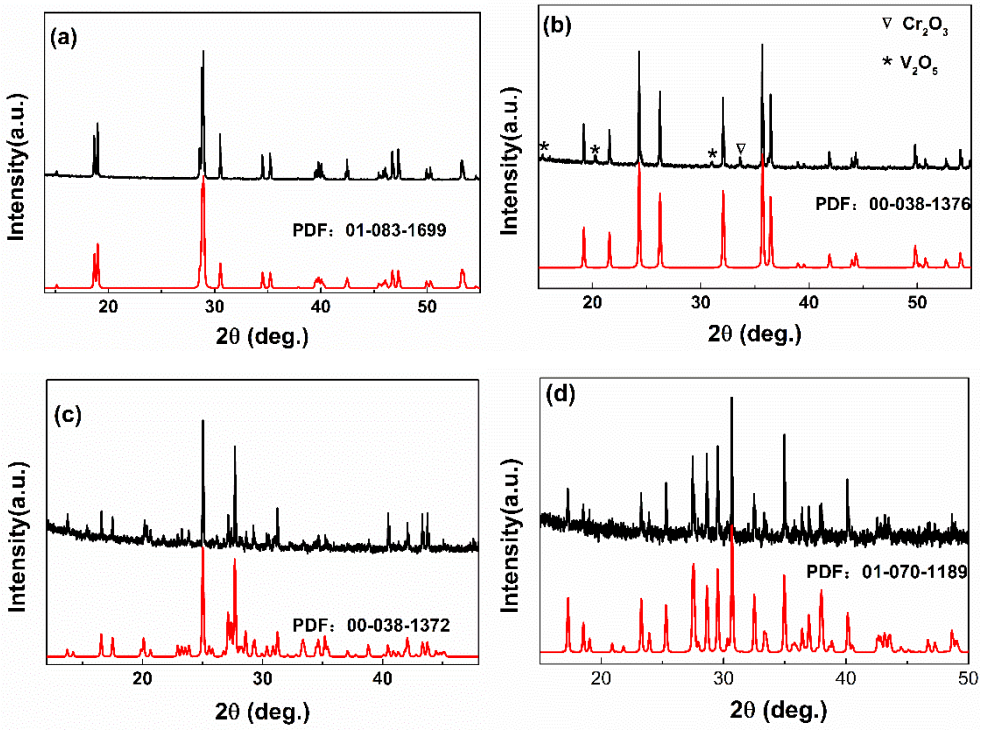

Figure 1. X-ray diffraction pattern of (**a**) $BiVO_4$, (**b**) $CrVO_4$, (**c**) $FeVO_4$, and (**d**) $Co_2V_2O_7$.

To visualize the coordination number associated with the structural transitions, crystal structures of monoclinic ($BiVO_4$, $Co_2V_2O_7$), triclinic ($FeVO_4$), and orthorhombic ($CrVO_4$) systems with polyhedral representation were drawn using a VESTA software as shown in Figure 2 (the "atomic coordinates" were obtained come from the joint conferences on pervasive computing (JCPC) references). The $BiVO_4$ crystal structure was monoclinic. From Figure 2a,b, Bi and V atoms occupied the symmetry position 4e, and O atoms occupied 8f. The distance between the V and O atoms was evenly distributed (approximately 1.68 Å and 1.785 Å); however, the distance of the Bi and O was very variable. There are six symmetry VO_4 tetrahedras and asymmetrical BiO_6 octahedra in one primitive cell of $BiVO_4$. The $CrVO_4$ crystal structure was orthorhombic (Figure 2c,d). The distance between the V and O atoms (approximately 1.63342 Å and 1.70978 Å) was shorter than that of $BiVO_4$, and the distances between the Cr and O atoms were 1.98422 Å and 2.04868 Å. It can be seen that there are four CrO_6 octahedra around each tetrahedron; however, each CrO_6 octahedron is not only connected with six tetrahedron vertices, but also connected with two other octahedron edges. The $FeVO_4$ crystal structure was triclinic Figure 2d. For $FeVO_4$, there were 18 symmetrical inequivalent atoms in a one-unit cell, and all the atoms occupied the symmetry position 2i (Figure 2e). The total number of atoms in a unit cell was 36. The distance between the V atom and the O atom was different. The unit cell contained three asymmetrical inequivalent VO_4 tetrahedra, two asymmetrical inequivalent FeO_6 octahedra, and one FeO_5 polyhedron [20] (Figure 2f). The CoV_2O_7 crystal structure was monoclinic Figure 2g, the total number of atoms in a unit cell was 44. The distance between the V atom and the O atom was different. The unit cell contained three symmetrical VO_4 of each tetrahedron and six asymmetrical CoO_6 octahedra (Figure 2h). It can be seen that each VO_4 tetrahedron was connected to four CoO_6 octahedra by the O atom; however, each CrO_6 octahedron was connected by the O atom to six VO_4 tetrahedras and shared a common edge with two other octahedral.

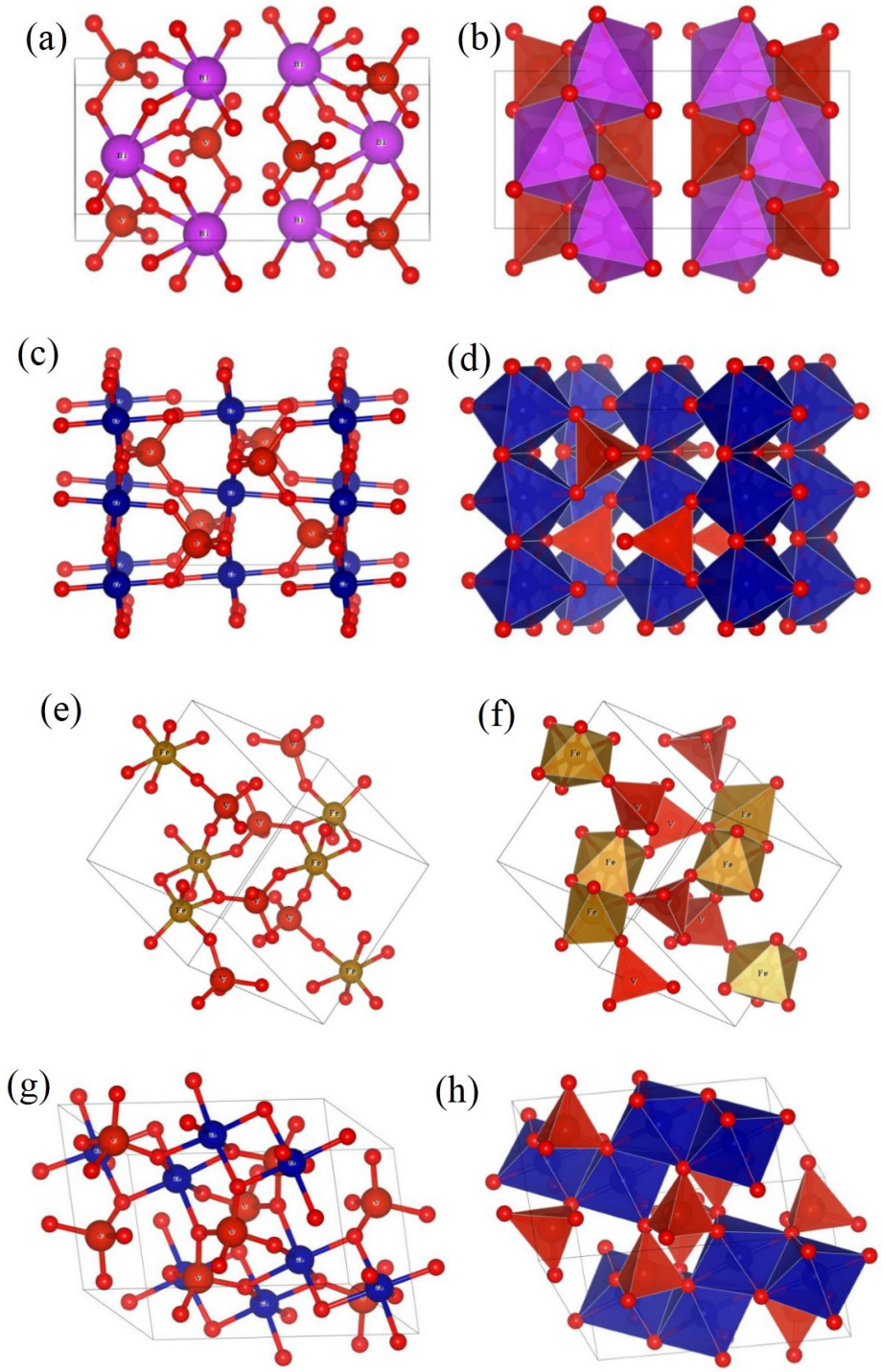

Figure 2. Crystal structure of (**a**,**b**) $BiVO_4$, (**c**,**d**) $CrVO_4$, (**e**,**f**) $FeVO_4$, and (**g**,**h**) $Co_2V_2O_7$.

3.2. Thermal Expansion Property

Figure 3 shows the relative linear thermal expansion of $BiVO_4$, $FeVO_4$, and $Co_2V_2O_7$. It was found that the samples have different relative linear thermal expansion. For $BiVO_4$, there was a thermal expansion inflection point at about 237 °C which means that the material occurs phase transition at the temperature. The coefficients of thermal expansion (CTEs) were calculated as the average linear thermal expansion coefficient in terms of the slope of thermal expansion versus temperature. The CTEs were measured to be $(4.664 \pm 0.005) \times 10^{-6}$ °C^{-1} (25–235 °C) and $(15.40 \pm 0.002) \times 10^{-6}$ °C^{-1} (240–550 °C). For $FeVO_4$, there was a gradual change thermal expansion at approximately 400 °C,

the CTE of $FeVO_4$ was obtained to be (2.751 ± 0.004) × 10^{-6} °C^{-1} from 20 to 350 °C and (5.245 ± 0.005) ×10^{-6} °C^{-1} from 400 to 600 °C. Although both vanadium and iron are variable metals and thermal expansion is related to valence states [21], we prepared and measured the material in an air atmosphere, vanadium and iron should remain stable in the highest valence state. So, there should be no chemical expansion here. The thermal expansion of $Co_2V_2O_7$ was stable below 500 °C, and the CTE was (9.230 ± 0.004) × 10^{-6} °C^{-1} from 20 to 500 °C. The inflection point above 500 °C is due to the softening of glass state above 500 °C which can be explained by the fact that $Co_2V_2O_7$ goes from the crystalline form to a glassy one. This phenomenon indicates that material intelligent stability exists with below 500 °C. Though the structure of $Co_2V_2O_7$ is similar to $BiVO_4$, their CTE is very different. This could come from the different ionic radius of Co^{3+} (63 pm) and Bi^{3+} (108 pm). The ionic radius of Co^{3+} (63 pm) equals that of Fe^{3+} (64 pm); however, they had the largest difference in CTE in this study. This was due to the different structures.

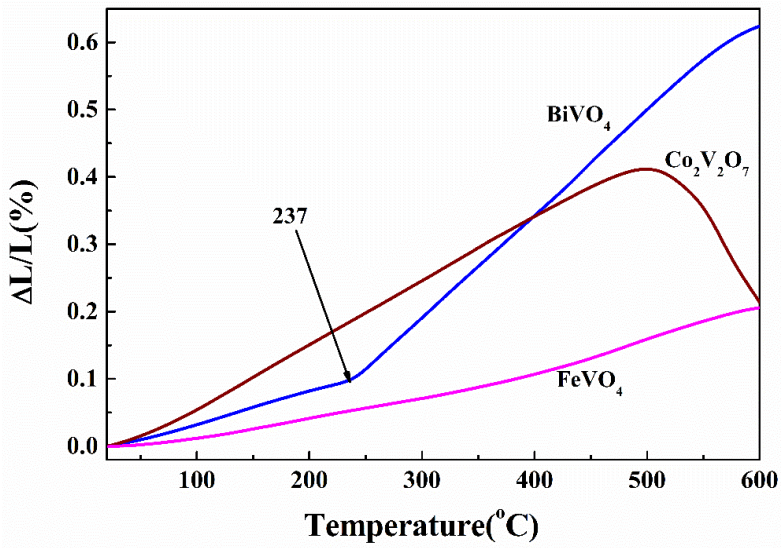

Figure 3. Relative length change of $BiVO_4$, $FeVO_4$, and $Co_2V_2O_7$.

Raman spectroscopy was applied to further demonstrate the existence of crystal. Raman spectra collected at room temperature is shown in Figure 4. The Raman spectra of $BiVO_4$, $CrVO_4$, $FeVO_4$, and $Co_2V_2O_7$ were in agreement with literature [10,20,22,23] and the spectra did not show the characteristic bands of V_2O_5. Hence, no effort was taken to consider the product selectivity in this work. For $BiVO_4$, the primitive cell contained 28 atoms (Figure 2) and, in principle, 81 vibrational modes were expected. The band at approximately 828 cm^{-1} corresponded to stretching modes of V–O bonds, and there was no splitting which means that degeneracy occurs in the symmetric stretching vibration of VO_4 tetrahedron. The strongest peak of $CrVO_4$ and $FeVO_4$ was much higher, whereas the stretching modes of V–O give rise to intense bands, the difference in electronegativity of these metal (Bi, Co, Cr, and Fe). The Raman bands of $FeVO_4$ were much more than that of $BiVO_4$, $CrVO_4$ and $Co_2V_2O_7$, because the structure of $FeVO_4$ is triclinic, and all vibrations are nondegenerate. The 36 atoms in the unit cell had 105 vibrational modes among which 54 optical modes were Raman active A_g modes, 51 were infrared active A_u modes [23]. For all Raman spectra, the stretching modes of V–O combining M–O and V–O occurred above 650 cm^{-1}, and bending modes together with stretching modes appeared in the 630–420 cm^{-1} region. The lower wavenumber bands were external modes from lattice, translational, and vibrational motions [24,25]. From a crystalline perspective, all catalysts were composed of V–O polyhedrons and other metal–oxygen polyhedrons.

In order to study the sudden change in thermal expansion of $BiVO_4$, the Raman spectroscopy dependent temperature of $BiVO_4$ is shown in Figure 5. The Raman bands became weaker and weaker with the increasing temperature which reflects the increase of the degree of disordering of the crystal structure. The relative intensity of 368 and 324 cm^{-1} had obvious change at 200 °C, and

they disappeared at 300 °C; meanwhile, there was a new band at approximately 345 cm^{-1}. There was not only one change. The bands at 127 and 211 cm^{-1} gradually became a wave packet; meanwhile, the 703 cm^{-1} band disappeared, and the 828 cm^{-1} band moved to 815 cm^{-1}, this might be caused by the bond expansion and weakening. All these mean that there was a phase transition between 200 °C and 300 °C. There was no change in the Raman spectra above 300 °C. The high temperature Raman spectra were in agreement with tetragonal structure which means that $BiVO_4$ crystal tetragonal as well [26]. Compared with Figure 3, we found that materials with high symmetry have larger CTE. The Raman band at 368 and 324 cm^{-1} could inhibit the thermal expansion of material. It means that the thermal expansion property was related to the structure of the material.

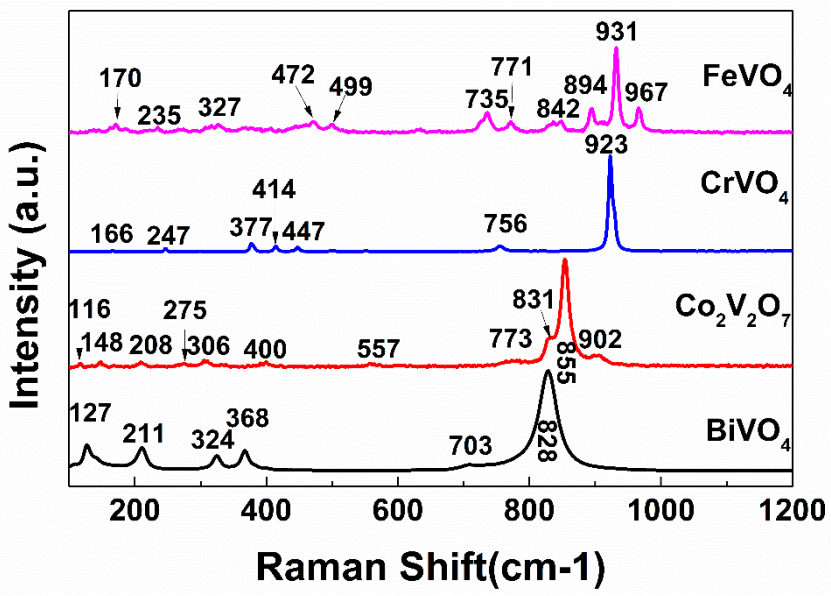

Figure 4. Raman spectra of $BiVO_4$, $FeVO_4$, $CrVO_4$, and $Co_2V_2O_7$.

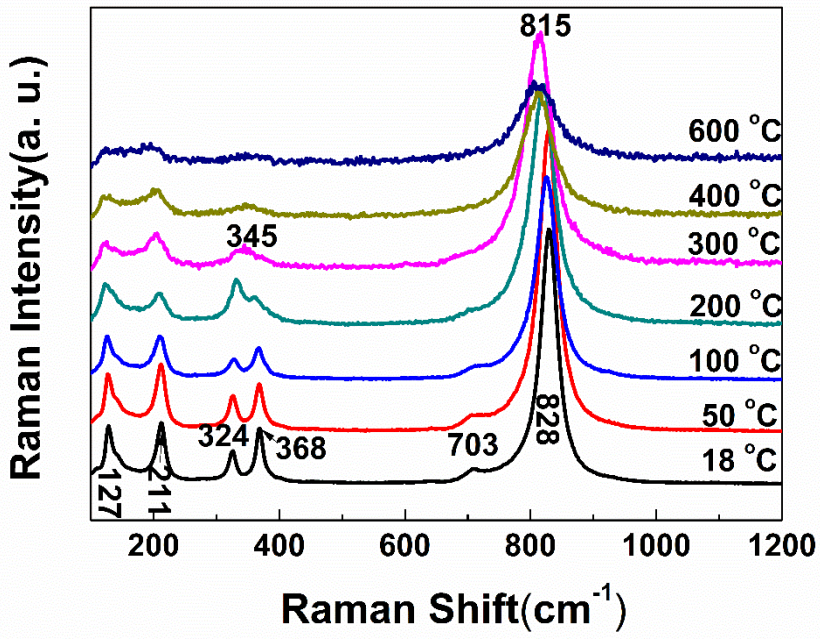

Figure 5. Raman spectra of $BiVO_4$ at temperature of 18, 50, 100, 200, 300, 400, and 600 °C.

4. Summary

Vanadium compounds were synthesized to investigate the thermal expansion properties and structure. The CTE of $Co_2V_2O_7$ was bigger than monoclinic structure $BiVO_4$ which means that the thermal expansion property was related to the ionic radius of metals. The CTE of the tetragonal structure of $BiVO_4$ was 15.27×10^{-6} °C^{-1} which was the biggest CTE in our measurement results, and the CTE of tetragonal structure $FeVO_4$ was 2.84×10^{-6} °C^{-1} which was the smallest. This indicates that the thermal expansion property was related to the structure of the material.

Author Contributions: Conceptualization, X.H. and C.Z.; methodology, X.H.; software, D.T.; validation, X.H., C.Z. and D.T.; formal analysis, D.T.; investigation, X.H.; resources, X.H.; data curation, C.Z.; writing—original draft preparation, X.H.; writing—review and editing, X.H.; visualization, X.H.; supervision, X.H.; project administration, X.H.; funding acquisition, X.H. All authors have read and agreed to the published version of the manuscript.

Funding: This research was funded by the Henan Province Education "The 13th Five-Year Plan" Project of Year 2016, grant number 2016-JKGHA-0017, and the Open Fund of Key Laboratory of Water-saving Agriculture of Henan Province, grant number FIRI2016-19-01.

Conflicts of Interest: The authors declare no conflict of interest.

References

1. Liu, C.; Su, J.; Zhou, J.; Guo, L. A Multi-step Ion Exchange Approach for Fabrication of Porous $BiVO_4$ Nanorod Arrays on Transparent Conductive Substrate. *ACS Sustain. Chem. Eng.* **2016**, *4*, 4492–4497. [CrossRef]
2. Huang, Z.F.; Pan, L.; Zou, J.J.; Zhang, X.; Wang, L. Nanostructured bismuth vanadate-based materials for solar-energy-driven water oxidation: A review on recent progress. *Nanoscale* **2014**, *6*, 14044–14063. [CrossRef]
3. Xu, J.; Wang, W.Z.; Wang, J.; Liang, Y.J. Controlled fabrication and enhanced photocatalystic performance of $BiVO_4$@CeO_2 hollow microspheres for the visible-light-driven degradation of rhodamine B. *Appl. Surf. Sci.* **2015**, *349*, 529–537. [CrossRef]
4. Wu, J.M.; Chen, Y.; Pan, L.; Wang, P.H.; Cui, Y.; Kong, D.C.; Wang, L.; Zhang, X.W.; Zou, J.J. Multilayer monoclinic $BiVO_4$ with oxygen vacancies and V^{4+} species for highly efficient visible-light photoelectrochemical applications. *Appl. Catal. B Environ.* **2018**, *221*, 187–195. [CrossRef]
5. Sleight, A.W.; Chen, H.-Y.; Ferretti, A.; Cox, D.E. Crystal growth and structure of $BiVO_4$. *Mater. Res. Bull.* **1979**, *14*, 1571–1581. [CrossRef]
6. Robertson, B.; Kostiner, E. Crystal structure and miissbauer effect investigation of $FeVO_4$. *J. Solid State Chem.* **1972**, *4*, 29–37. [CrossRef]
7. Lopez-Moreno, S.; Errandonea, D.; Pellicer-Porres, J.; Martinez-Garcia, D.; Patwe, S.J.; Achary, S.N.; Tyagi, A.K.; Rodriguez-Hernandez, P.; Munoz, A.; Popescu, C. Stability of $FeVO_4$ under Pressure: An X-ray Diffraction and First-Principles Study. *Inorg. Chem.* **2018**, *57*, 7860–7876. [CrossRef]
8. Sim, D.H.; Rui, X.H.; Chen, J. Direct growth of $FeVO_4$ nanosheet arrays on stainless steel foil as high-performance binder-free Li ion battery anode. *RSC Adv.* **2012**, *2*, 3630–3633. [CrossRef]
9. Liu, X.L.; Cao, Y.C.; Zheng, H.; Chen, X.; Feng, C.Q. Synthesis and modification of $FeVO_4$ as novel anode for lithium-ion batteries. *Appl. Surf. Sci.* **2017**, *394*, 183–189. [CrossRef]
10. Ghani, F.; Raza, A.; Kyung, D.G.; Kim, H.S.; Lim, C.J.; Nah, I.W. Optimization of synthesis conditions of high–tap density $FeVO_4$ hollow microspheres via spray pyrolysis for lithium–ion batteries. *Appl. Surf. Sci.* **2019**, *497*, 143718. [CrossRef]
11. Yan, N.; Xu, Y.; Li, H.J.; Chen, W. The preparation of $FeVO_4$ as a new sort of anode material for lithium ion batteries. *Mater. Lett.* **2016**, *165*, 223–226. [CrossRef]
12. Li, J.; Zhao, W.; Guo, Y.; Wei, Z.; Han, M.; He, H.; Yang, S.; Sun, C. Facile synthesis and high activity of novel $BiVO_4$/$FeVO_4$ hetero junction photocatalyst for degradation of metronidazole. *Appl. Surf. Sci.* **2015**, *351*, 270–279. [CrossRef]
13. Wang, M.; Liu, Q.; Zhang, D. Synthesis and photocatalytic property of V_2O_5/$FeVO_4$ composite novel photocatalyst. *Adv. Mater. Res.* **2011**, *129–131*, 784–788.
14. Baran, E.J. Materials belonging to the $CrVO_4$ structure type: Preparation, crystal chemistry and physicochemical properties. *J. Mater. Sci.* **1998**, *33*, 2479–2497. [CrossRef]

15. Wu, F.F.; Yu, C.H.; Liu, W.X.; Wang, T.; Feng, J.K.; Xiong, S.L. Large-scale synthesis of $Co_2V_2O_7$ hexagonal microplatelets under ambient conditions for highly reversible lithium storage. *Mater. Chem. A* **2015**, *32*, 16728–16736. [CrossRef]
16. Sun, H.; Chen, X.; Chai, H.; Wang, Y.C.; Jia, D.Z.; Cao, Y.L.; Liu, A.J. 3D porous hydrated cobalt pyrovanadate microflowers with excellent cycling stability as cathode materials for asymmetric supercapacitor. *Appl. Surf. Sci.* **2019**, *469*, 118–124. [CrossRef]
17. Ji, W.H.; Sun, Y.C.; Kumar, C.M.N.; Li, C.; Nandi, S.; Jin, W.T.; Su, Y.; Sun, X.; Lee, Y.; Harmon, B.; et al. Non-collinear magnetic structure and anisotropic magnetoelastic coupling in cobalt pyrovanadate, $Co_2V_2O_7$. *Phys. Rev. B* **2019**, *100*, 134420. [CrossRef]
18. Wachowski, S.; Kamecki, B.; Winiarz, P.; Dzierzgowski, K.; Mielewczyk-Gryń, A.; Gazda, M. Tailoring structural properties of lanthanum orthoniobates through an isovalent substitution on Nb-site. *Inorg. Chem. Front.* **2018**, *5*, 2157–2166. [CrossRef]
19. Errandonea, D.; Manjón, F.J. Pressure effects on the structural and electronic properties of ABX_4 scintillating crystals. *Prog. Mater. Sci.* **2008**, *53*, 711–773. [CrossRef]
20. Bera, G.; Reddy, V.R.; Rambabu, P.; Mal, P.; Das, P.; Mohapatra, N.; Padmaja, G.; Turpu, G.R. Triclinic–monoclinic–orthorhombic (T–M–O) structural transitions in phase diagram of $FeVO_4$-$CrVO_4$ solid solutions. *J. Appl. Phys.* **2017**, *122*, 115101. [CrossRef]
21. Løken, A.; Ricote, S.; Wachowski, S. Thermal and Chemical Expansion in Proton Ceramic Electrolytes and Compatible Electrodes. *Crystals* **2018**, *8*, 365. [CrossRef]
22. Wang, N.L.; Qiu, J.; Wu, J.; You, K.Y.; Luo, H.A. A comparison of the redox properties of bulk vanadium mixed oxide catalysts. *Catal. Lett.* **2015**, *145*, 1792–1797. [CrossRef]
23. Zhang, A.M.; Liu, K.; Ji, J.T.; He, C.Z.; Tian, Y.; Jineng, F.; Zhang, Q.M. Raman phonons in multiferroic $FeVO_4$ crystals. *Chin. Phys. B* **2015**, *24*, 126301. [CrossRef]
24. Yuan, H.L.; Yuan, B.H.; Li, F.; Liang, E.J. Phase transition and thermal expansion properties of $ZrV_{2-x}P_xO_7$. *Acta Phys. Sin.* **2012**, *22*, 226502.
25. Liang, E.J.; Liang, Y.; Zhao, Y.; Liu, J.; Jiang, Y.J. Low-frequency phonon modes and negative thermal expansion in $A(MO_4)_2$ (A = Zr, Hf and M = W, Mo) by Raman and Terahertz time-domain spectroscopy. *J. Phys. Chem. A* **2008**, *112*, 12582–12587. [CrossRef]
26. Yu, J.; Kudo, A. Effects of Structural Variation on the Photocatalytic Performance of Hydrothermally Synthesized $BiVO_4$. *Adv. Funct. Mater.* **2006**, *16*, 2163–2169. [CrossRef]